AUT Journal of Mechanical Engineering

AUT J. Mech. Eng., 7(4) (2023) 367-388
DOI: 10.22060/ajme.2024.22716.6071

Investigating the Effect of Casing Injection Parameters on Transonic Axial Compressor Performance

Sarallah Abbasi [1]*, Mohammad Raiszadeh Oskoui [2]

[1] Department of Mechanical Engineering, Arak University of Technology, Arak, Iran
[2] Department of Mechanical Engineering, Sharif University of Technology, Tehran, Iran

ABSTRACT: One of the factors that can cause a reduction in the efficiency and performance of axial compressors is the tip leakage flow of the compressor blade. In the first, the compressor's performance curve is compared with experimental results obtained under the condition of no air injection, and a statistically significant agreement is observed. The present study investigates the impact of various parameters, including flow rate, diameter, angle, and injection location, on the compressor's performance curve and flow structure, taking into account the injection of air into a passage. The results indicate that the compressor's stall margin and stable range extension are at their maximum values at a specific scale of each of the aforementioned parameters. Any deviation from this scale, either by reducing or increasing the injection parameters, leads to a reduction in the above characteristics. Although the presence of injection leads to an increase in the total pressure ratio in all injection states compared to the state without injection, the adiabatic efficiency at similar mass flow rates exhibits no significant change. The results also indicate that flow injection in the most suitable state increases the stall margin amount by 27% and the stable range extension of the compressor by 192.

Review History:

Received: Oct. 01, 2023
Revised: Mar. 03, 2024
Accepted: May, 17, 2024
Available Online: Jun. 13, 2024

Keywords:

Axial Compressor
Numerical Simulation
Air Injection
Tip Leakage Flow
Stall

1- Introduction

The axial flow compressor is a critical component of gas turbine engines that greatly influences their performance and stability [1]. The existence of an area in these rotary machines, between the blade tip and engine shell, is inevitable. Research has emphasized the significant impact of blade tip leakage flow on compressor performance. The collision of the main flow with the tip leakage flow leads to vortex formation on the blade surface, increasing blockage in the fundamental flow passage and reducing compressor efficiency. Undoubtedly, the presence of areas with thermodynamic and aerodynamic drops and the formation of vortex flow in these regions are detrimental to compressor performance. Considering the extensive use of compressors across various industries, controlling blade tip leakage flow is crucial for minimizing losses and optimizing compressor efficiency [2-6].

A study was carried out by Chunill et al. to investigate the impact of a significant tip gap on an axial compressor. Their results indicated that an increase in the tip gap size led to a reduction in blockage resulting from tip leakage flow [7]. Xiaodong Ren et al. investigated the flow structure within the blade tip gap of an axial compressor and its flow blockage. Their observations indicated that the compressor flow structure was influenced by tip leakage flow under varying performance conditions, leading to reduced performance [8]. In their research, Wisler et al. reported that doubling the size of the tip gap in a compressor results in a 1.5 percent reduction in its total efficiency [9]. Similarly, Wiseman and colleagues found that reducing the size of the tip gap leads to a significant decrease in fuel consumption [10]. Wilke et al. conducted a numerical study to investigate the flow characteristics of a compressor in both design and off-design conditions. The results of their simulation indicated that the behavior of tip leakage flow, design velocity, and attack angle in the blade tip are the main factors affecting the compressor's flow stability. Specifically, they found that increasing the attack angle near the blade tip can cause flow separation in the blade suction area under off-design conditions. In light of these findings, they developed a modified shell compatible with NASA Rotor 37 [11]. Davis et al. conducted a study to investigate stall formation in a transonic axial compressor rotor, utilizing both numerical and experimental methods. In their study, Davis et al. found that drops caused by tip leakage vortexes become more severe in a near-stall state [12]. Zhang et al. conducted a numerical study to investigate the formation and impact of acquiring waves [13]. Adamczyk et al. also conducted a numerical investigation into the role of tip gap in a near stall condition of an axial fan with a high pace and suggested that the interaction between the tip leakage vortex and the inlet impact wave can play a significant role in a fan's flow performance [14]. Additionally, Wilke et al. studied the impact of axial cracks on the flow field in a transonic rotor

*Corresponding author's email: s_abbasi@arakut.ac.ir

blades row. They proposed a modified shell conFig.uration that could reduce the power of the tip leakage vortex and its impact on the flow inside the passage [15].

The utilization of numerical and simulation software has become increasingly prevalent due to the time-consuming and expensive nature of experimental tests, as well as the limitations of some laboratory tools. A variety of methods have been developed to control tip leakage flow and prevent the occurrence of stalls. The first method involves using professional design tools to create a sufficient stall margin, ensuring a safe operating range for the compressor's performance, and maintaining axial flow [16-20]. The second method involves utilizing stall warning [21-25] and stability control [26-28] after the compressor design process. These methods can be categorized into two types: passive controlling and active controlling. In the passive controlling method, tip leakage flow is controlled by modifying the geometrical shape of the blade and shell. On the other hand, energy is applied using different techniques, such as airflow injection, in the active controlling method to control tip leakage flow [29].

Vuong et al. conducted a study on the passive controlling method, specifically investigating the effects of a recirculation channel and casing treatment involving a peripheral groove type in a compressor shell. Their findings indicated a significant increase in the stall margin area by up to 42%, with the lowest possible reduction in efficacy [30]. In a separate study, Li et al. investigated the use of a new hybrid casing treatment in an axial flow compressor. Their study revealed that the hybrid slot-groove treatment can improve the stall margin by 19.79% while resulting in a 1.5% decrease in efficiency [31].

Epstein was the first numerical researcher to suggest an active controlling method to address compressor instability [32]. In recent years, with the development of computational capabilities, many studies have been conducted to increase axial compressor efficiency using the active controlling method. One approach is the use of air tips to increase the stall margin. One of the earliest studies was conducted by Koch et al. in the late 1960s, which focused on controlling flow instabilities through the application of air blows and suction [33, 34]. In another investigation, Tong et al. studied the effect of tip injection on delaying rotational stall in a centrifugal compressor [35]. Khaleghi et al. conducted a numerical simulation to examine the effects of air tip injection using a rotary inlet in a single-rotor row. Their findings demonstrated that recirculating a small mass amount in the compressor can expand the margin stall [36].

In another study, Liu et al. calculated the promotion of stall margin through injection usage in an axial compressor. They observed that forming a small axial distance between the injection location and the rotor leading edge and increasing injection speed can be beneficial in

the stall margin [37]. Li et al. investigated Self-adaptive stability-enhancing technology with tip air injection in an axial flow compressor. The results showed that the proposed self-adaptive stability control using a digital signal processing controller can save energy when the compressor is stable [38]. Yang et al. studied air injection near the blade leading edge in an axial compressor, focusing on compressor performance charts in different injection angles. They found that an injection angle of approximately 20% (relative to the inlet flow direction) resulted in a greater increase in the compressor function value [39].

Li et al. investigated the effects of Self Recirculating injection in an axial flow compressor. They observed that injection can improve the stall margin by 13.67% and 13% in single- and three-stage axial flow compressors, respectively, with no efficiency penalty and with only a small fraction of the injected momentum ratio recirculated near stall [40]. In another study, Zhang et al. conducted experimental and numerical investigations on tip injection in a subsonic flow compressor. They varied the height of the injection tube opening from 2 to 6 times the rotor tip gap and the peripheral coverage from 8.3% to 25% of the total perimeter of the compressor. Their results showed that maximum stability development is achieved when the injectors are choked, and the effect of the injector peripheral coverage percentage on compressor stability depends on the height of the injection throat in an unchoked injector, and vice versa [41].

Beheshti et al. conducted a study on tip injection with a casing treatment to enhance the performance of an axial compressor. They found that the stall margin could be increased by up to 7% [42]. In another research, Beheshti et al. proposed a new design for injection in axial compressors, which involved direct injection to a high-pressure gas jet using a peripheral groove near the blade tip. They repeated the process for three flow rates and observed that the defined stall margin for the highest flow rate (4.35% of the main flow rate) increased by roughly 14% [43]. Meanwhile, Mushtaq et al. investigated the impact of injection parameters such as angle and flow rate on the performance of an axial compressor. Their findings showed that increasing the injection angle and flow rate could lead to an increase in pressure ratio and compressor function. They conducted their study by creating a peripheral injection [44]. The body of research on this topic demonstrates that various flow-controlling methods can significantly impact the performance of a compressor. However, a review of the literature reveals that the majority of studies have focused on tip injections in subsonic compressors, with few investigations conducted on transonic compressors. Moreover, most researchers have primarily concentrated on examining the effect of injection on the compressor curves' function and stall margin changes. As a result, there has been relatively less investigation into the flow behavior and characteristics of transonic compressors, including tip leakage flow, main flow, and boundary layer, in the presence of impact waves.

This article provides a comprehensive analysis of the impact of various injection parameters, such as flow rate, diameter, angle, and distance from the blade leading edge, on the overall performance of the compressor. Notably, the study includes a detailed investigation of the injection impact at different locations, particularly the distance from

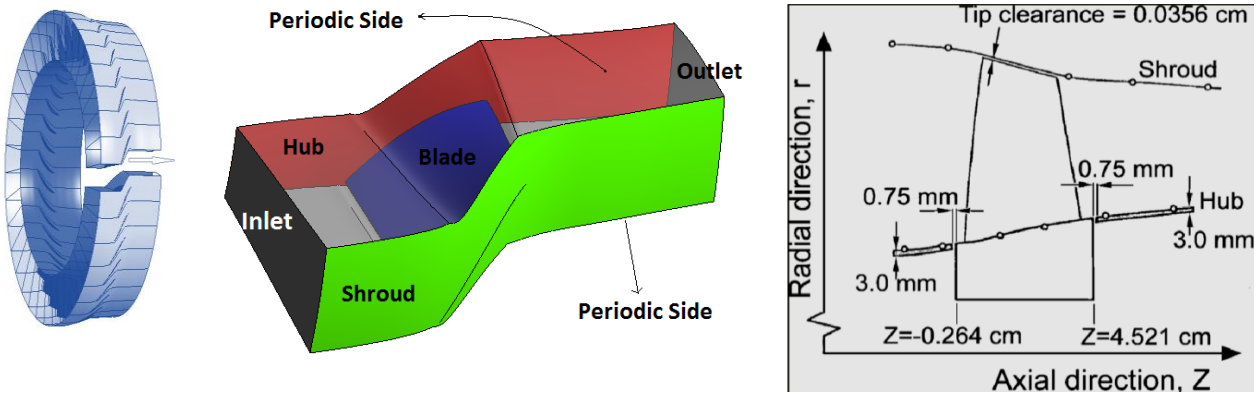

Fig. 1. Geometry of the rotor 37 without injection

Table 1. Characteristics of rotor 37 [3]

PARAMETERS	DESIGN VALUE
Number of Rotor Blades	36
Rotor Wheel Speed, rpm	17188.7
Rotor Tip Speed. m/s	454.14
Rotor Aspect Ratio	1.19
Rotor Total Pressure Ratio	2.106
Rotor Adiabatic Efficiency	0.877
Flow Coefficient	0.453
Mass Flow, kg/s	20.188

the injection location to the blade leading edge, a factor that has not been extensively discussed in most other articles. The study employs a unique approach using a cylindrical pipe with one injection tube placed on each passage. This method contrasts with that of most other articles, which typically involve piercing part of the compressor casing, resulting in a change in its shape, and injecting the flow in a strictly peripheral manner or using a method other than a cylindrical tube. Ultimately, the study evaluates the impact of this active control technique on the compressor's performance and the flow field under the specified conditions.

2- The compressor of NASA Rotor 37 Simulation

2- 1- Computational Geometry

The object of study in this article is NASA Rotor 37, a transonic axial compressor that was designed and tested at the NASA Research Center. Various studies on this rotor have been conducted by several researchers, and numerous laboratory reports have been published about it. Fig. 1 provides an overview of NASA Rotor 37, while Table 1 presents some of its key characteristics [2, 3]. Due to the fact that the information about the axial compressor, including the geometry, test conditions, and performance characteristics of the compressor is very little and mostly incomplete. Therefore, researchers are forced to use this rotor. Therefore, according to the existence of this information for NASA Rotor 37, this rotor has been used for research.

The dimensions and geometries of the blade's various parts were obtained from NASA's reports in this study, numerical analysis was carried out using a passage modeling approach to reduce computational time and expenses. Each passage consists of three parts: rotor inlet, rotor blade, and

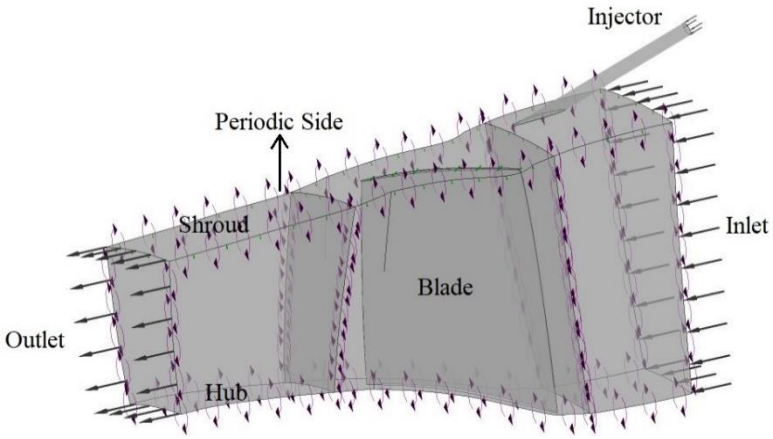

Fig. 2. Boundary conditions in a rotor 37 passage with injection

rotor outlet. Fig. 2 provides a general view of NASA Rotor 37 in a rotor passage with the addition of an injection duct. As noted in the introduction, instead of using peripheral injection (as in Fig. 3-a) [45], a cylindrical tube (as shown in Fig. 3-b) was used, which presents the schematic view of the injection tube characteristics. Details of the investigated parameters are presented in Table 2, including reference parameters such as injection intensity (mass flow rate ratio of injected mass flow to compressor mass flow rate), diameter, angle, and injection location (relative to the length of the tip chord), which are 0.87%, 2 mm, 30 degrees, and 41.17%, respectively.

No specific criteria were established for the injection parameter amounts in this research. Instead, an estimated range was considered for these parameters based on the results of previous studies [38-41, 46, 47]. The impact of different parameters on compressor performance was subsequently explored, with each parameter's amount being changed in each step, and its impact being evaluated to determine the best amount. Once the optimal value for one parameter was determined, the other parameters were examined in turn. Thus, the parametric study investigated the impact of mass flow rate, injector diameter, injector angle, and injector location, respectively.

2- 2- Grid Generation and Independence of the Results from the Grid

The grid generation for the compressor was performed using ANSYS Turbo Grid in a structured form. To achieve this, each passage was divided into 30 sections in the radial direction, 69 sections in the tangential direction, and 100 sections in the axial direction. The tip gap distance was further divided into 12 segments, resulting in a structured grid. The grid density near the walls was designed such that the value of $y+$ was less than 5, and the computational domain of a passage contained 290,514 computational cells.

To ensure the accuracy of the meshing and the number of grids, the independence of the results from the number of grids was examined. For this purpose, the compressor performance was evaluated using eight different types of meshing, as outlined in Table 3. Fig. 5 shows a diagram plotted based on the number of cells and pressure ratio. The results indicate that increasing the number of elements from 290,000 computational cells to 500,000 computational cells did not result in noticeable changes in the compressor's performance characteristics. However, the desired values changed when the grid numbers increased from 150,000 computational cells to 290,000 computational cells. Accordingly, a grid of 290,000 elements was deemed suitable for the current research. (It is proportionally augmented in all three directions.)

2- 3- Solving Settings

ANSYS CFX software was utilized as the solver in this research, using the finite volume method to solve governing Eqs such as momentum, continuity, and energy. This solver can analyze three-dimensional and viscous flows. The k-ω-SST two-Eq. turbulence model was used to estimate viscosity and derive Reynolds stresses. As shown in Fig. 1, the inlet boundary conditions were set to an overall temperature of 15 degrees Celsius and a pressure of 1 atmosphere. At the outlet boundary, a static pressure distribution was applied using the radial equilibrium condition. The adiabatic wall was subjected to a no-slip boundary condition, while the periodic boundary condition was applied to the sides of the solving domain. The casing and blade walls were subject to conditions of adiabatic and perpendicular flow inlet to the surface. The intensity of the inlet free flow turbulence was considered to be insignificant, at about 2 percent. As per Fig. 3 and Table 2, the mass flow rate at the pipe inlet boundary of injection was determined. Additionally, the inlet temperature of the injection flow was considered to be 300 Kelvin. A frozen rotor was applied as the common condition between the tube and shell at the outlet of the injection tube

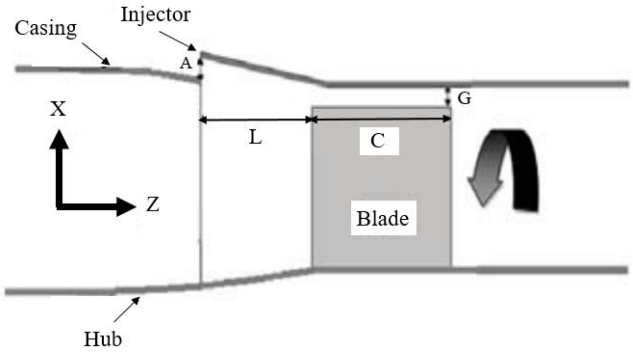

(a) [44]

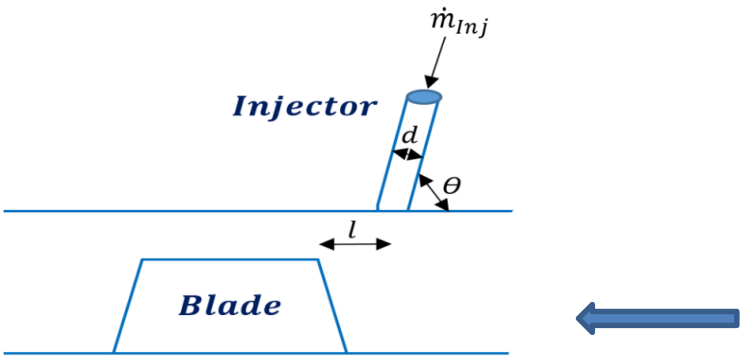

(b)

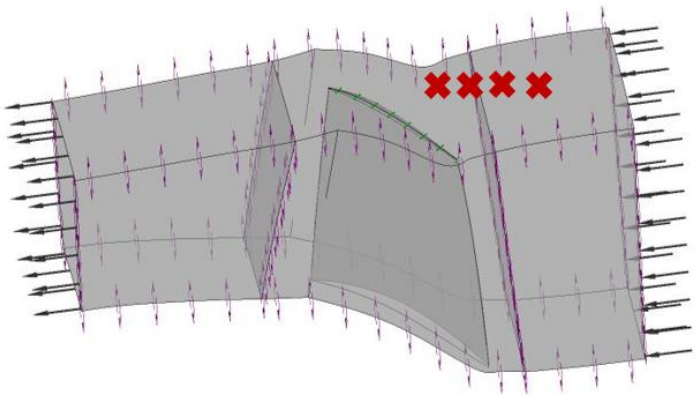

(c)

Fig. 3. (a) Schematic view of peripheral injection (b) Schematic design from injection tube characteristics (c) The injection location

Table 2. Injection tube characteristics

$I = \dot{m}_{inj} / \dot{M}$ (%)	d (mm)	θ (degree)	$S = l / c$(%)
0.87	2	15	8.85
1.73	3	22	25.02
2.6	4	30	41.17
3.47	5	38	61.82

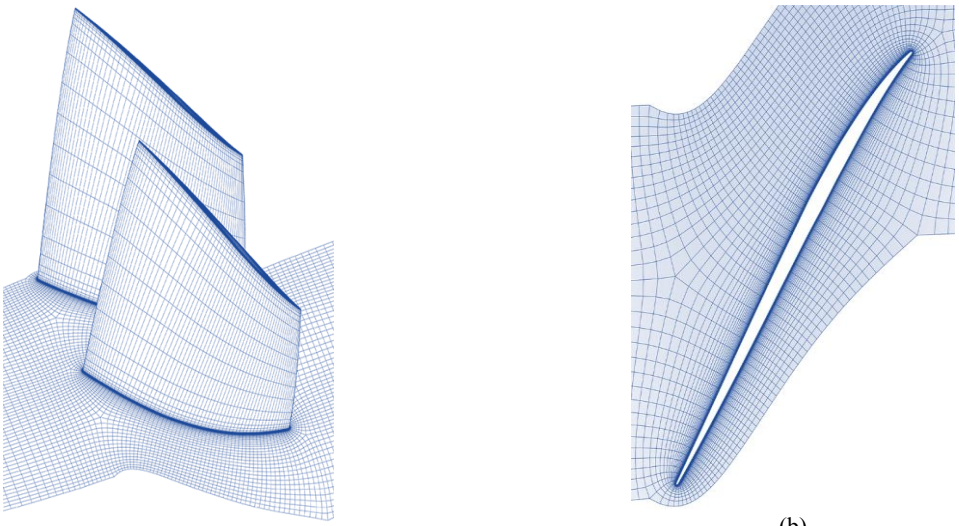

(a) (b)

Fig. 4. The grid generation of the rotor blade (a) the whole three-dimensional blade (b) in the blade tip zone

Table 3. Different modes of meshing examine the independence of the results from grids

Total Pressure Ratio	Number of Nodes	Number of Cells
2.023	172318	158474
2.0269	221295	204778
2.0292	269946	250898
2.0373	310386	290514
2.0368	368292	344656
2.037	419043	393440
2.0371	478901	449250
2.03705	532372	499879

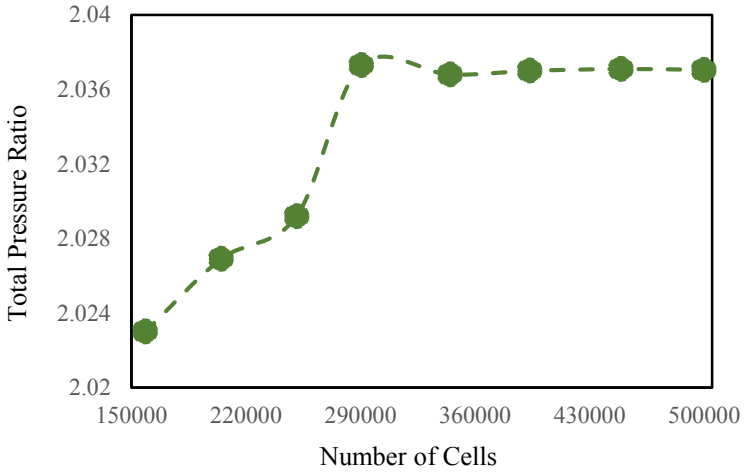

Fig. 5. Independence of solving from the number of computational cells

Table 4. RAM and CPU od PC

Processor	Intel(R) Core(TM) i7-4510U CPU @ 2.00GHz 2.60 GHz
RAM	8.00 GB

boundary. The no-slip boundary condition was also applied to the adiabatic wall of the injection tube. The performance of $k-\omega$ the SST turbulence model in simulations with reverse pressure gradient and ultrasonic waves is better than other models of its family. Also, the SST turbulence model is among the best two-Eq. models for transition calculation. The main idea of K-Omega SST is to combine SKW in the region near the wall with SKE outside the boundary layer. In fact, the K-omega SST model is a combination of K-Epsilon and K-Omega turbulence models.

The specifications of CPU and PC RAM used are listed in Table 4. Also, when running the software, three CPU cores were used, which took approximately 30-40 minutes for each run.

In this research, ANSYS CFX software is selected as a solver. This software uses the finite volume method to solve the governing Eqs including momentum (Eq 1), continuity (Eq 2), and energy (Eq 3).

$$\frac{\partial(\rho u_i)}{\partial t}+\frac{\partial \rho u_i u_j}{\partial x_j}=-\frac{\partial \rho}{\partial x_i}+\frac{\partial \tau_{ij}}{\partial x_j} \quad (1)$$

$$\frac{\partial \rho}{\partial t}+\frac{\partial \rho u_i}{\partial u_j}=0 \quad (2)$$

$$\frac{\partial(\rho E)}{\partial t}+\frac{\partial \rho H u_j}{\partial x_j}= \frac{\partial}{\partial x_j}(u_i \tau_{ij})-\frac{\partial}{\partial x_j}((\frac{u_l}{\mathrm{Pr}}+\frac{u_t}{Pr_t})\frac{\partial T}{\partial x_j}) \quad (3)$$

where ρ is the density, u_i is the velocity component along the x_i direction, p is the pressure, T is the temperature, and E is the total energy. μ_l and μ_t are the smooth and turbulent viscosity coefficients, respectively Pr , and Pr_t are the calm and turbulent Prantel numbers, respectively. Viscous stress tensor τ_{ij} , strain rate tensor s_{ij} and total enthalpy H are as follows:

$$\tau_{ij}=2(u_l+u_t)(s_{ij}-\frac{1}{3}s_{kk}\delta_{ij}) \quad (4)$$

$$s_{ij} = \frac{1}{2}\left(\frac{\partial u_i}{\partial x_j} + \frac{\partial u_j}{\partial x_i}\right) \tag{5}$$

$$H = E + \frac{P}{\rho} \tag{6}$$

Also, the effect of turbulence fluctuations has been considered using the shear stress transport (SST) $k-\omega$ turbulence model. The Eq.s of turbulent kinetic energy transfer k and turbulence-specific dissipation rate ω are written as follows:

$$\frac{\partial(\rho k)}{\partial t} + \frac{\partial(\rho u_j k)}{\partial x_j} = \frac{\partial}{\partial x_j}\left[(\mu_l + \sigma_k \mu_t)\frac{\partial k}{\partial x_j}\right] + P_k + \beta^* \rho \omega k \tag{7}$$

$$\frac{\partial(\rho\omega)}{\partial t} + \frac{\partial(\rho u_j \omega)}{\partial x_j} = \frac{\partial}{\partial x_j}\left[(\mu_l + \sigma_\omega \mu_t)\frac{\partial \omega}{\partial x_j}\right] + P_\omega - \beta\rho\omega^2 + 2(1-f_1)\frac{\rho\sigma_{\omega 2}}{\omega}\frac{\partial k}{\partial x_j}\frac{\partial \omega}{\partial x_j} \tag{8}$$

where P_k and P_ω are terms of k and ω, respectively, and are defined as follows:

$$P_k = \mu_t \Omega^2, P_\omega = c_\omega \rho \Omega^2 \tag{9}$$

where Ω represents the magnitude of the vortex. μ_t is the eddy viscosity, which is defined as follows:

$$\mu_t = \frac{a_1 \rho k}{\max(a_1\omega, f_2 \|\Omega\|)} \tag{10}$$

σ_k, σ_ω, β and c_ω are constant values that are calculated by the following formula:

$$\varphi = f_1\varphi_1 + (1-f_1)\varphi_2 \tag{11}$$

The function f_1 and f_2 is calculated as follows:

$$f_1 = \tanh(\Gamma_1^4), f_2 = \tanh(\Gamma_2^4) \tag{12}$$

$$\Gamma_1 = \min[\max(\frac{500\mu_l}{\rho\omega D^2}, \frac{\sqrt{k}}{0.09\omega D}), \frac{4\rho\sigma_{\omega 2}k}{CD_{k\omega}D^2}] \tag{13}$$

$$CD_{k\omega} = \max(2\frac{\rho\sigma_{\omega 2}}{\omega}\frac{\partial k}{\partial x_j}\frac{\partial \omega}{\partial x_j}, 1\times10^{-20}) \tag{14}$$

$$\Gamma_2 = \max(\frac{2\sqrt{k}}{0.09\omega D}, \frac{500\mu_l}{\rho\omega D^2}) \tag{15}$$

where D is the wall distance, a_1 is a constant value of 0.31 and k is equal to 0.41.

The set of fixed values of coefficients φ_1 and φ_2 is as follows:

$$\varphi_1 : \partial k_1 = 0.85, \partial\omega_1 = 0.5, \beta_1 = 0.075, C\omega_1 = 0.53 \tag{16}$$

$$\varphi_2 : \partial k_2 = 1, \partial\omega_2 = 0.85, \beta_2 = 0.0828, C\omega_2 = 0.44 \tag{17}$$

2- 4- Validation of the Results

To ensure the accuracy of the results, the findings of this study were compared with experimental results in the existing NASA document [3] and also numerical result reference [39], and their validation was verified. Performance curves of the compressor were derived as pressure ratio vs. mass flow rate and adiabatic efficiency vs. mass flow rate diagrams, as shown in Fig. 6. The comparison between the present numerical simulation results and the experimental results showed a satisfactory level of agreement. The average error is calculated from Eq. 18, which is 4.35% and 1.13% for pressure and efficiency, respectively.

$$Error = (EXP\_result - NUM\_result) \div EXP\_result \tag{18}$$

3- Results

3- 1- Performance Curves in Different Injection Conditions

To investigate the impact of tip injection parameters on transonic compressor performance, and to compare their effects through numerical analysis, performance curves in the form of pressure ratio vs. mass flow rate and adiabatic efficiency vs. mass flow rate were plotted for different injection states, as shown in Figs. 7 and 8, respectively.

As illustrated in Fig. 7-A, the best conditions for compressor performance in terms of lower mass flow rates with no occurrence of stall or decreased pressure ratio were observed at injection intensities of 2.60% and 3.47%. The impact of different injection diameters on lower mass flow rates (Fig. 7-B) showed the optimum diameters to be 3mm, 2mm, 4mm, and 5mm, respectively. Similarly, examining the impact of injection angle (Fig. 7-C) revealed that injection angles of 30 and 38 degrees had the best impact

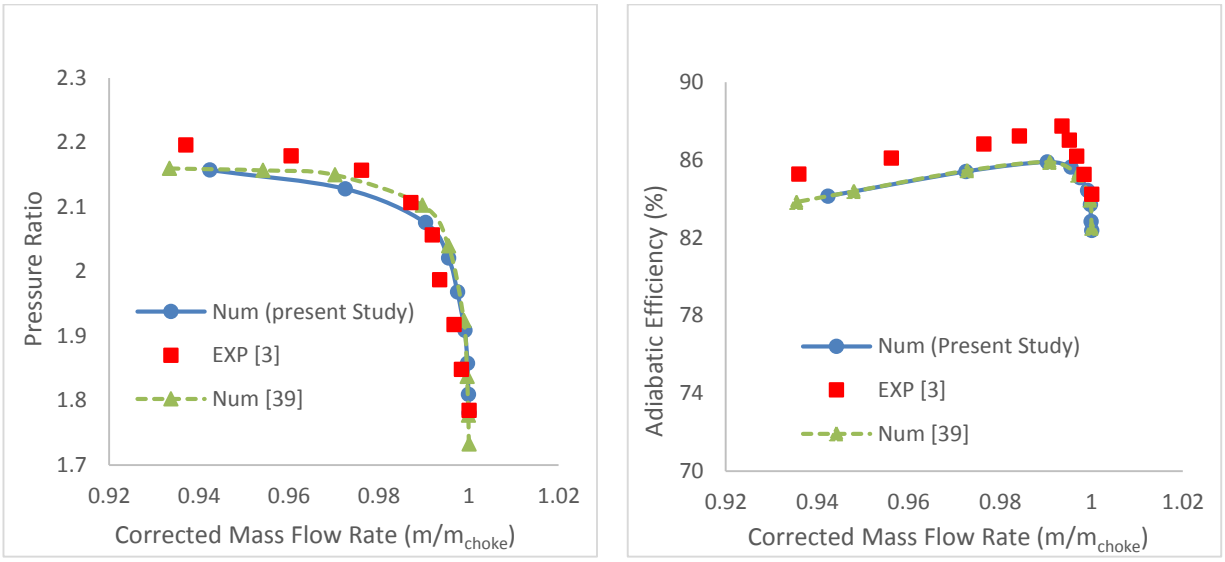

(a) (b)

Fig. 6. Compressor performance curves: (a) pressure ratio vs. mass flowrate, (b) the adiabatic efficiency vs. mass flowrate

on compressor performance at lower mass flow rates, respectively. Moreover, the impact of injection angles of 15 and 22 degrees was found to be almost the same. The impact of injection location was also investigated, as shown in Fig. 7-D. The results indicate that at a distance ratio of 41.17% (the ratio of the injection distance from the leading edge to the length of the axial chord in the blade tip), the compressor is capable of stable performance at lower mass flow rates compared to other states. It was also observed that the maximum pressure ratio occurred at a distance ratio of 25.02%. However, when the other injection parameters (intensity, diameter, and angle) were optimized for the best mass flow rate ratio, the compressor was unable to operate efficiently at low flow rates. The locations of points A and B represent the performance flow rate in a near-stall state with no injection and the performance flow rate in a near-stall state with injection, respectively.

It is known that the operating range of the compressor is different in different modes and different values of the injection parameters. Especially, the effect of injection parameters shows itself at the beginning of the stall region (low mass flow conditions) and the left side of the functional diagram. In other words, the functional range of the compressor (the distance between the choke points and the near stall) and also the development of the stall margin are different in different values of the injection parameters. The difference values of these two parameters are shown in Figures 9 and 10.

Fig. 8 shows the comparison of compressor efficiency vs. mass flow rate in different injection conditions. The results indicate that, under the designed conditions, the efficiency remains constant or increases with the application of injection. As demonstrated in Fig. 7, the compressor's capability to operate near stall conditions improves with injection application at lower mass flow rates. The overall shape of the efficiency curve reveals a decrease in efficiency with a reduced mass flow rate. Thus, while a decrease in efficiency is important, it is considered to be of secondary importance compared to the stability of the compressor's performance at lower mass flow rates.

Correlations 19 and 20 are used to derive the amount of stall margin and stable range extension in the impact of injection in comparison to no injection state [43], [48].

$$SM = \left(\frac{\Pi_{stall} \times \dot{m}_{\eta \max}}{\Pi_{\eta \max} \times \dot{m}_{stall}} - 1\right) \tag{19}$$

$$SRE = \left(\frac{(\dot{m}_{choke} - \dot{m}_{stall})_{with\_Injection}}{(\dot{m}_{choke} - \dot{m}_{stall})_{without\_Injection}} - \frac{(\dot{m}_{choke} - \dot{m}_{stall})_{without\_Injection}}{(\dot{m}_{choke} - \dot{m}_{stall})_{without\_Injection}}\right) \times 100 \tag{20}$$

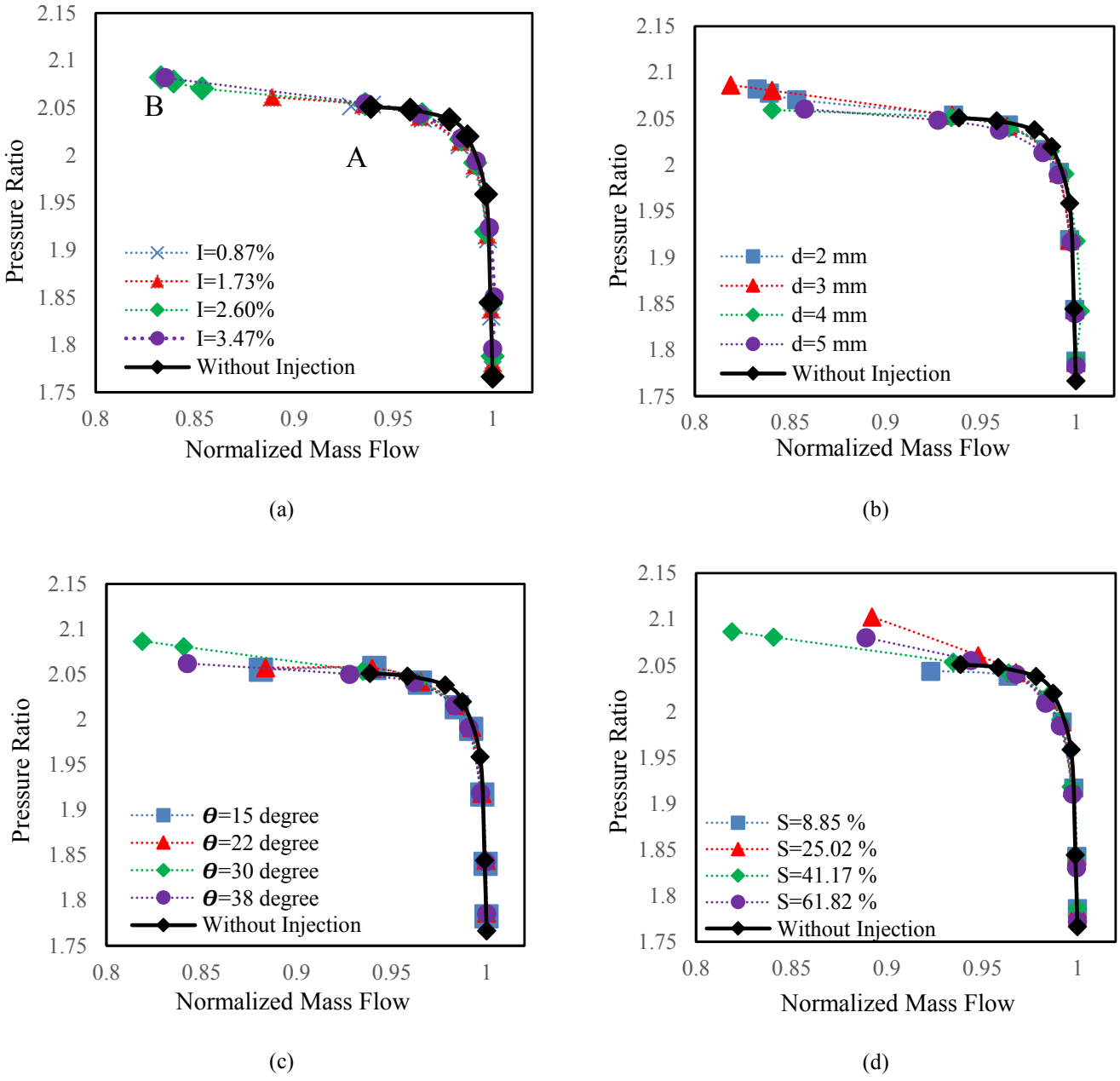

Fig. 7. The performance curves of pressure ratio vs. compressor mass flowrate in no injection and injection states in the parameters, (a) injection intensity, (b) injection diameter, (c) injection angle, (d) distance ratio

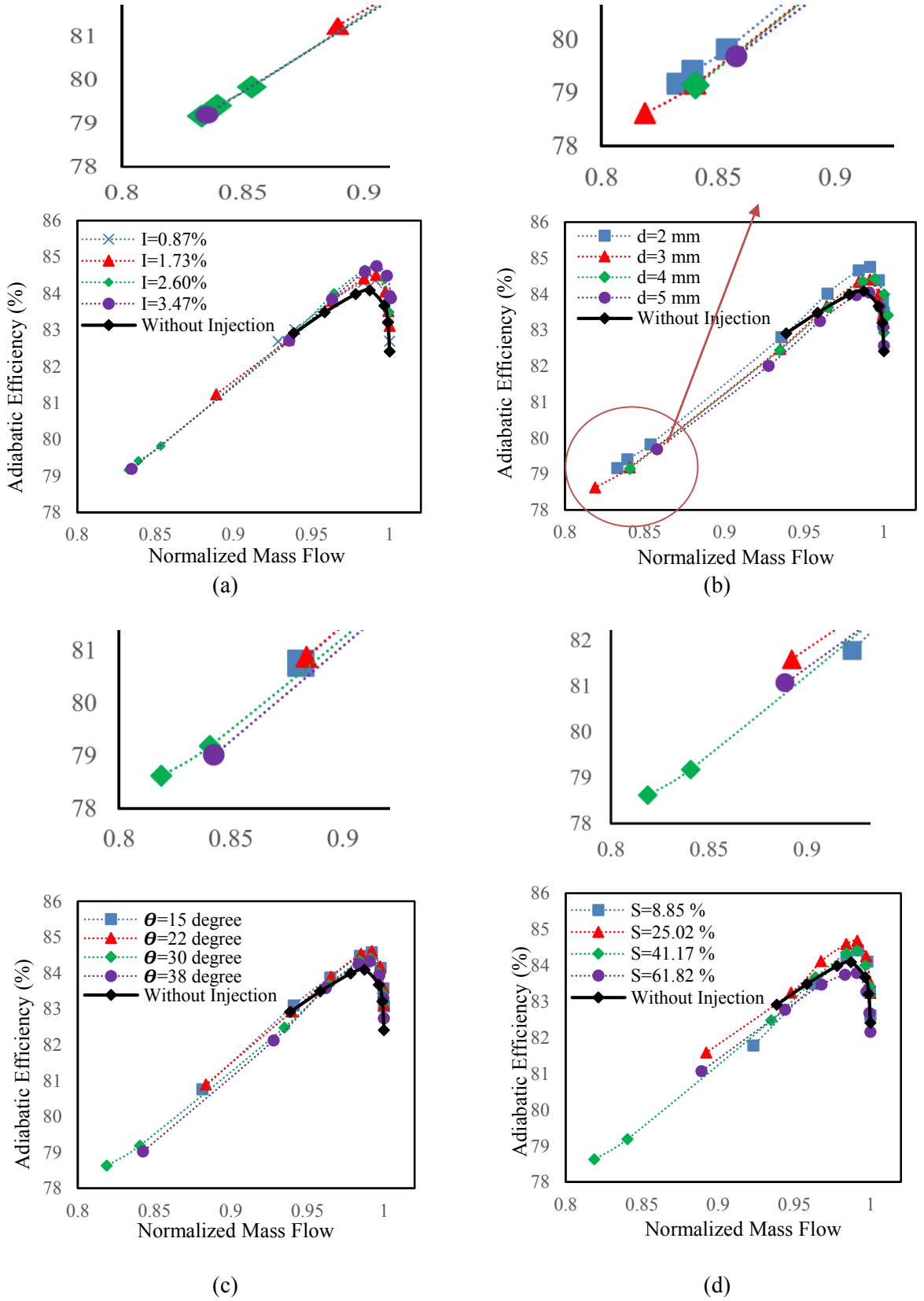

Fig. 8. Performance diagrams of adiabatic efficiency vs. mass flowrate in no injection and injection states in parameters (a) injection intensity (b) injection diameter (c) injection angle (d) distance ratio

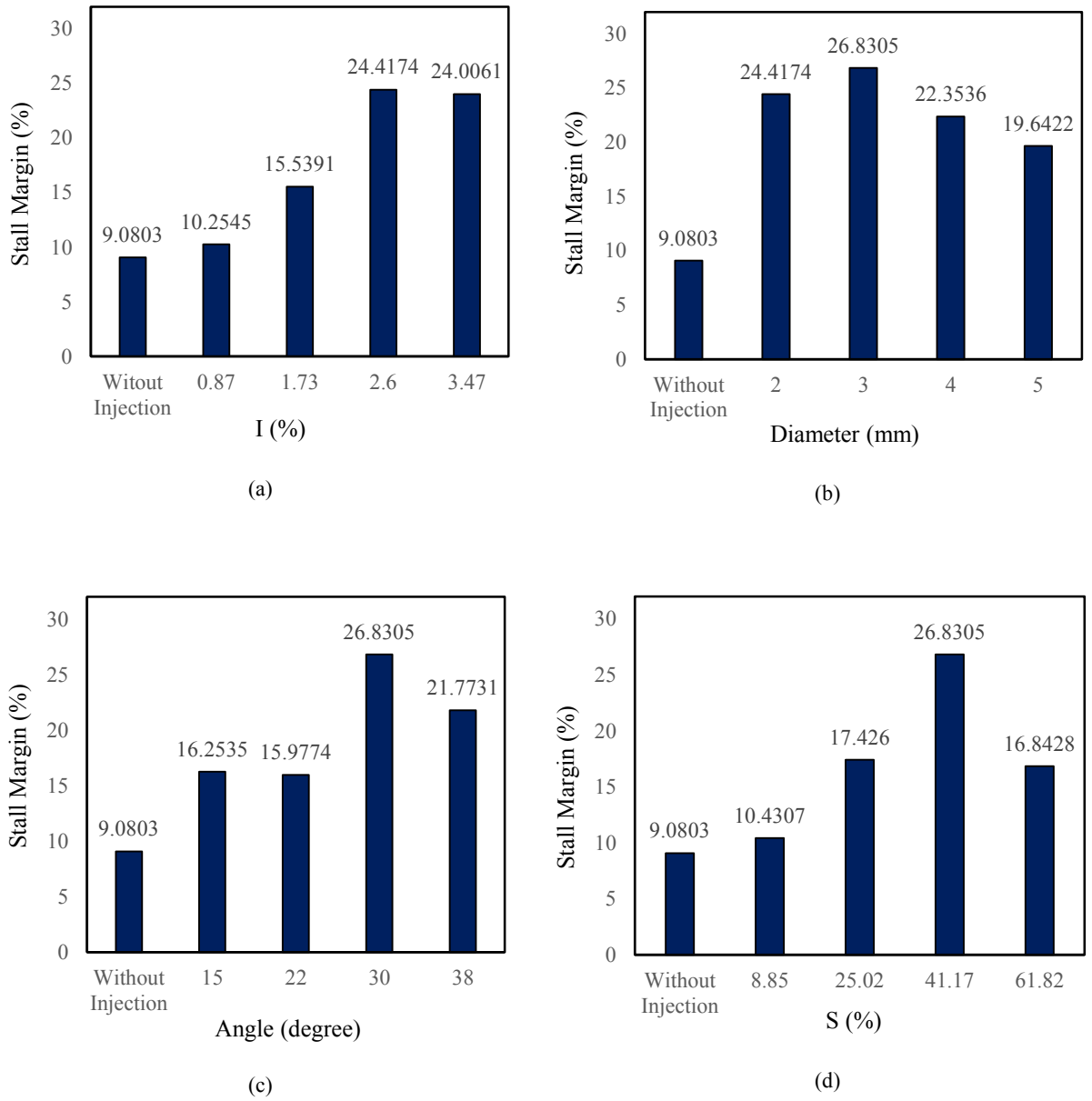

Fig. 9. Surveying the impact of injection parameters on stall margin (a) impact of injection intensity (b) injection diameter (c) injection angle (d) distance ratio

Fig.s 9-A and 10-A reveal that increasing injection intensity up to 2.6% leads to an increase in stall margin (SM) and stable range extension (SRE). However, further increasing the injection intensity results in a reduction in SM and SRE. The maximum values of SM and SRE occur at an injection intensity of 2.6%. Similar trends were observed for other injection parameters. For instance, the highest values of SM and SRE were observed at a 3mm injection diameter, as shown in Fig.s 9-B and 10-B. Decreasing or increasing the injection diameter reduced the positive impact of the injection.

Fig.s 9-C and 10-C demonstrate that injection angles of 15 and 22 degrees have nearly the same impact. Increasing the injection angle up to 30 degrees results in a higher increase in SM and SRE compared to the two previous angles. However, the increasing trend reverses by increasing the injection angle to 38 degrees. Regarding the injection distance from the compressor leading edge, SM and SRE increase by increasing the distance ratio up to 41.17%, but this trend reverses at a distance ratio of 61.82% (Fig.s 9-D and 10-D).

The results indicate that the injection parameters have different impacts on the development of compressor performance. Therefore, it cannot be concluded that an absolute increase or decrease in a certain parameter would always result in an increase or decrease in the compressor's function. Instead, each injection parameter has a specific

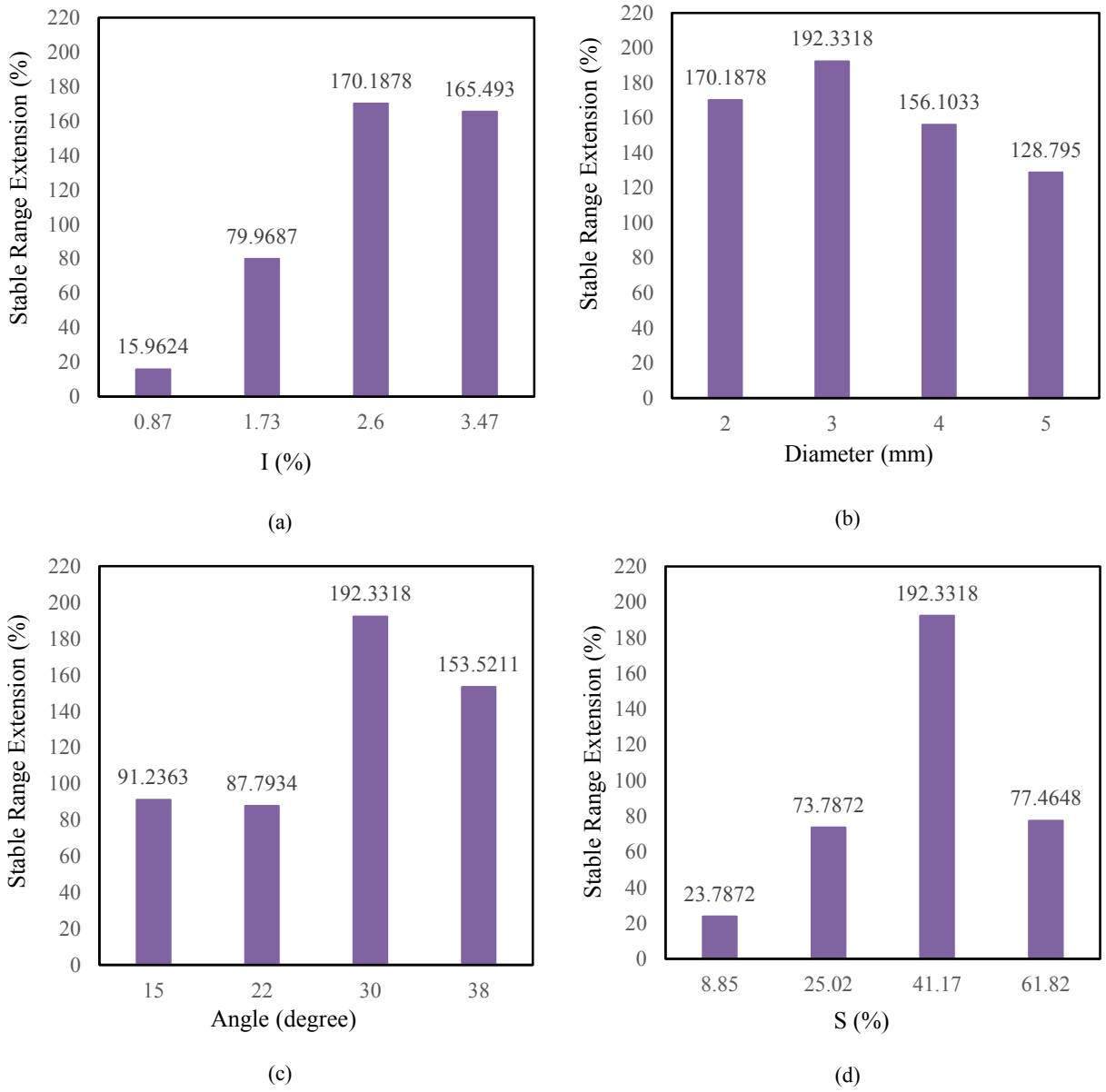

Fig. 10. Surveying the impact of injection parameters on stable range extension (a) impact of injection intensity (b) injection diameter (c) injection angle (d) distance ratio

suitable range that must be determined to optimize compressor performance. The impact of injection diameter on SM and SRE parameters is lower than other injection parameters. The difference in these parameters is 7% and 64% when the diameter is changed from 2mm to 5mm, respectively. However, this difference is 14% and 155% for the impact of injection intensity, respectively. The impact of changes in distance ratio on these parameters is higher than the impact of flow rate. According to the results of the parametric analysis, the most beneficial injection state for stable compressor performance at lower mass flow rates, increased SM, and higher SRE is an injection intensity of 2.6%, a diameter of 3mm, an angle of 30 degrees, and an injection location (distance ratio) of 41.17%. This injection state results in a 27% increase in SM and a 192% increase in SRE. It should be noted that a higher distance ratio of 25.02% has a better result than a distance ratio of 41.17% in terms of stable compressor performance.

With the increase in injection intensity, the value of SM and SRE increases due to the flow rate introduced through the injection tupe and pushed back into the shock zone. But it can be seen that if the flow intensity exceeds a certain limit, the injection flow can cause a shock on the main flow and reduce the functional stability of the compressor.

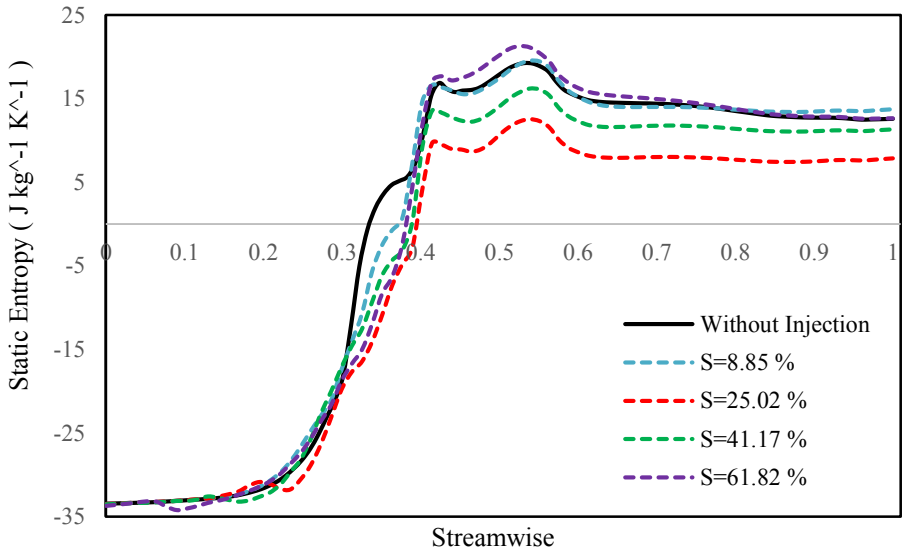

Fig. 11. The entropy curves in the span of 0.98 in the no injection state and in the injection state in different distance ratio

3- 2- Investigating the Flow Structure under Different Injection Locations

In the previous section, a comparison was made to examine the simultaneous impacts of various injection parameters. In this section, the focus is on studying the detailed structure of the flow resulting from changes in injection location. This is particularly important because the impact of injection location (distance ratio) has not been thoroughly investigated in previous studies. Fig. 11 illustrates the entropy chart for the flow with and without air injection (at different distances from the leading edge) at performance point A (the stall point in a no-injection state). Points A and B are the flow rate performance points in a near-stall state with no injection and with injection, respectively.

It is evident that the primary flow entropy before reaching the rotor blade is almost identical in all states. However, the entropy suddenly increases in all states when the flow reaches the rotor. In the no-injection state, this phenomenon occurs earlier than in the injection state (at distance ratios of 25.02% and 41.17%). Moreover, the increase in entropy is higher in the no-injection state than in the injection state. Specifically, the injection state at a distance ratio of 25.02% results in a higher increase in entropy than the injection state at 41.17%. It is evident that injecting at a distance ratio of 8.85% has a negligible impact compared to the no injection state. On the other hand, injecting at a distance ratio of 61.82% leads to an increase in entropy in the tip area and has a detrimental effect on the structure of the tip leakage flow.

Based on the above information, it can be inferred that no injection state leads to a stronger occurrence of the tip leakage flow, resulting in more drops than in the injection state at distance ratios of 25.02% and 41.17%, which can be considered acceptable. In other words, the increase in entropy is not solely due to shock waves but is also caused by tip leakage vortices generated by the interaction of the tip leakage flow and the main flow. Therefore, the appropriate injection of gas in the shell can weaken the shock waves and enhance the power of the tip leakage flow, subsequently reducing the power of the tip leakage vortex. Consequently, the flow drop is reduced by applying a suitable injection, leading to a decrease in entropy. Finally, the diagrams indicate that injecting gas too far or too close to the leading edge is not beneficial, as it can aggravate the conditions of the vortices and tip leakage flow, and is also ineffective.

Fig. 12 was used to examine and compare the flow structure details in the axial compressor. The results were obtained at different states, including static pressure in performance state A in no injection (Fig. 15a), and at various injection locations (Fig.s 15b to 15e) in a 0.98% span. The no-injection condition leads to the formation of a vortex structure in the flow lines within the tip gap zone, as observed in a near-stall performance state (A). This vortex formation in the flow passage causes blockage, and if it persists, it can negatively impact compressor performance. The application of injection effectively prevents the occurrence of recursive and vortex flow in all surveyed states except at a distance ratio of 61.82% (Fig.s 15b to 15d). In the absence of injection and at the performance state of A, an intersection between the main flow and tip leakage flow is observed near the rotor leading edge. This is due to an increase in the power of the tip

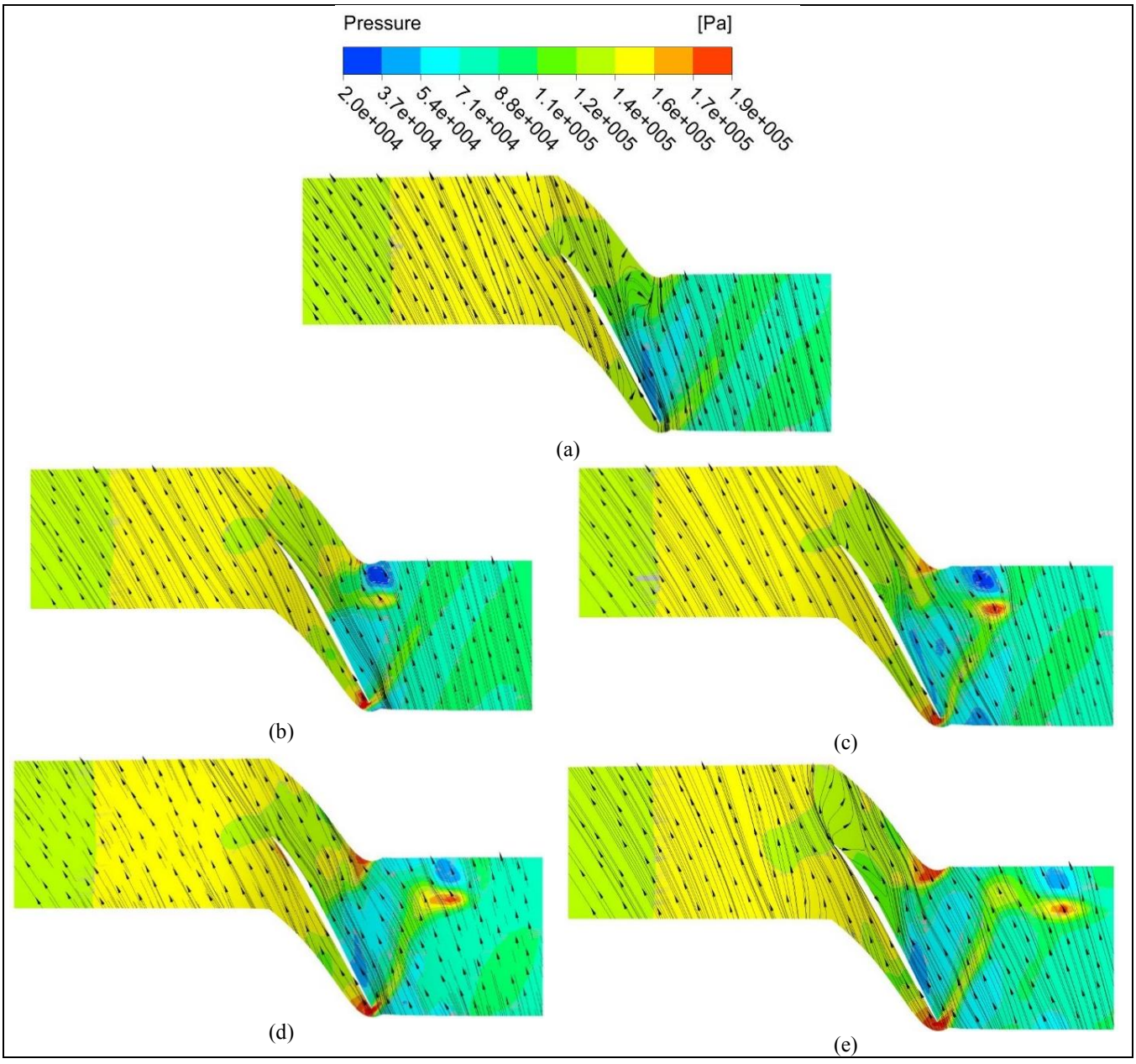

Fig. 12. Contour of static pressure distribution in 98% span along with flow lines in (a) no air injection state in the performances state of A, and in the state of with an air injection in the performance state of A, distance ratio : (b) 8.85% (c) 25.05% (d) 41.17% (e) 61.82%

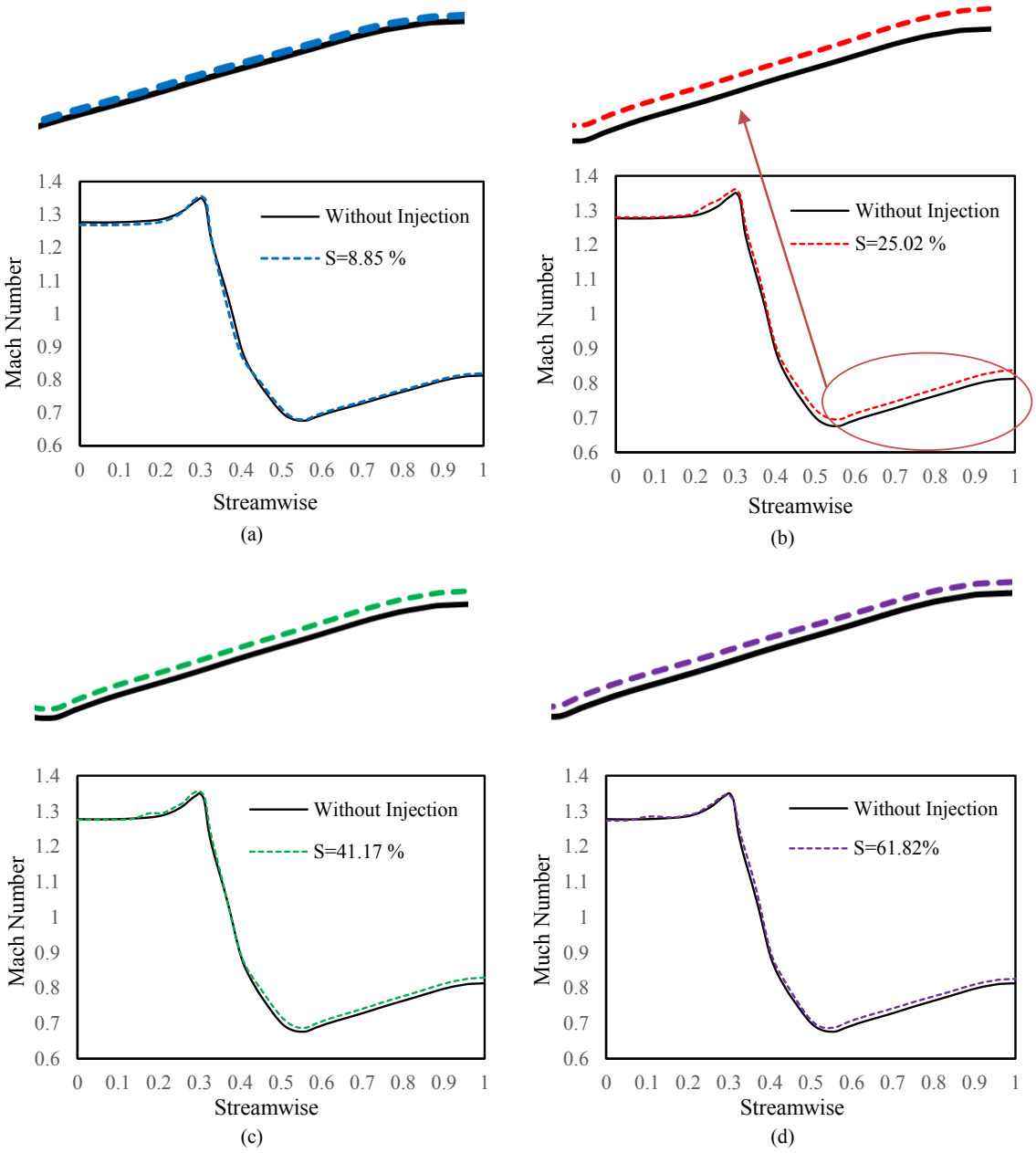

Fig. 13. The Mach number flow chart along the axial in without air injection and with air injection states at distance ratio: (b) 8.85% (c) 25.05% (d) 41.17% (e) 61.82%

leakage flow compared to the main flow in a near-stall state. However, in the investigated states, the power of the main leakage flow increases compared to the tip leakage flow, which prevents the occurrence of an intersection between the two flows at the rotor's leading edge. This phenomenon is achieved by injecting the flow from the tip and increasing the momentum of the main flow. Nevertheless, as shown in Fig. 15d, tip injection at a distance ratio of 61.82% does not help to unblock the main flow. In Fig. 15b (at a distance ratio of 8.85%), a slight deviation in the flow passage is observed, which is not present in injection states of 25.02% and 41.17% (Fig.s 15c and 15d). Therefore, injection at 25.02% and 41.17% states has a more positive effect compared to other states.

Fig. 13 shows the Mach flow curve along the axial direction in two conditions: with and without injection at the performance point of A, in different injection states. As observed, the Mach number abruptly decreases in both states

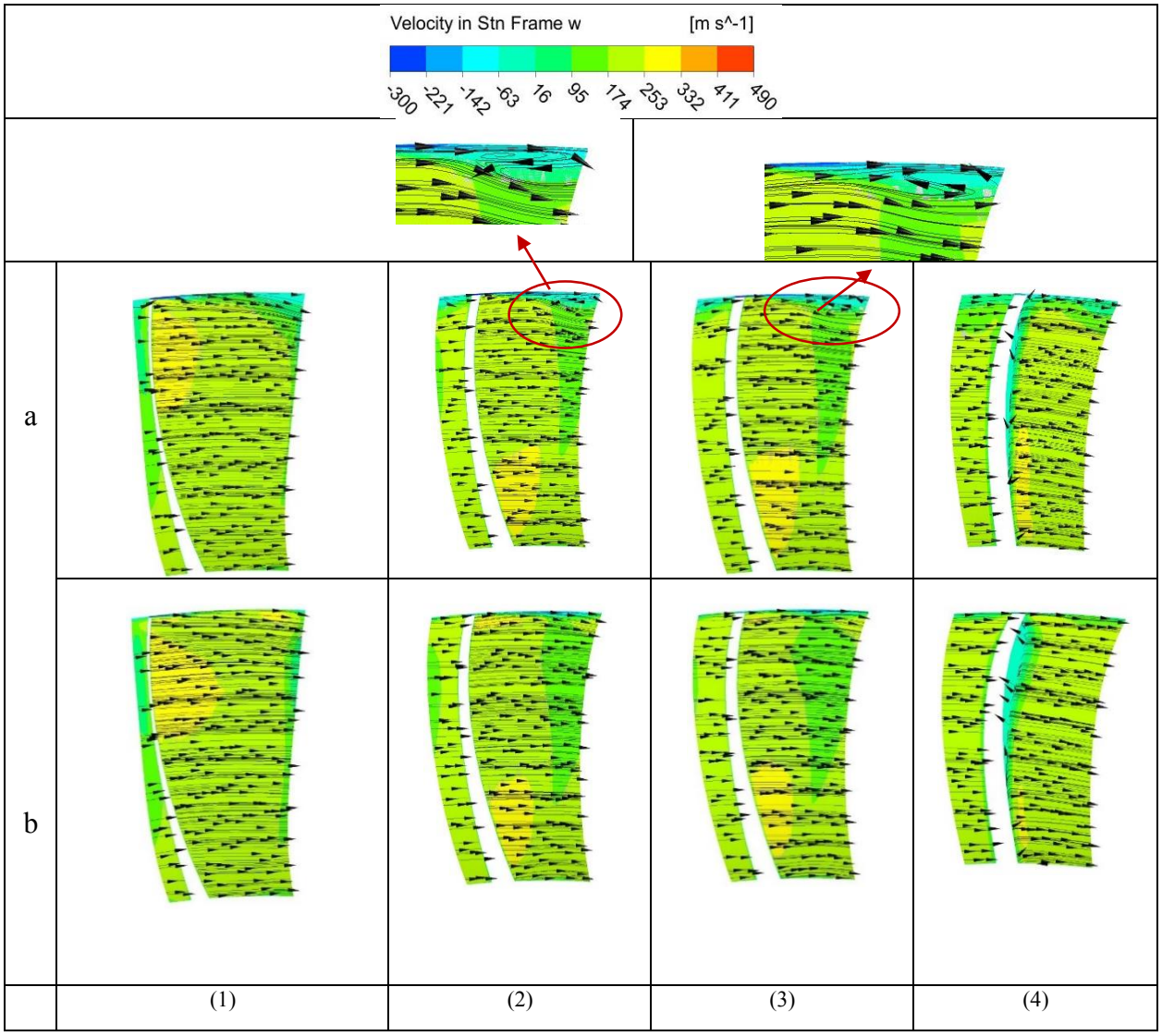

Fig. 14. The axial velocity contour at 5 locations of the blade at the performance point of A in the states: (a) Without injection, (b) With injection at CSL: (1) 31.5%, (2) 35%, (3) 36%, (4) 43%

due to the occurrence of dense shock waves in the tip area. However, applying injection reduces the power of the shock waves to some extent. A comparison of different injection states reveals that at the 25.02% injection state, the Mach number decreases less than in other modes due to the impact of the shock wave. This indicates a weakening of the power of the shock wave in the tip area. Consequently, the impacts of the shock wave confrontation with the boundary layer and leakage flow are reduced by decreasing the power of the shock wave in this injection state. This modification of the flow behavior in the tip area helps prevent recursive flow and flow segregation.

3- 3- Comparing the Effect of Tip Leakage Flow in the no Injection State and the Optimal Injection State

Fig. 14 presents the axial velocity contour in the absence of air injection and the optimal air injection states (injection intensity of 2.6%, diameter of 3mm, injection angle of 30 degrees, and distance ratio of 41.17%) in the performance state of A, at different planes along the flow. This was done to investigate the occurrence and distribution of stall cells both peripherally and radially. In the air injection state, no significant occurrence of recursive flow or vortex was observed, and the reduction of axial velocity only occurred in a small area near the blade tip. In contrast, investigating the axial velocity contour in the absence of air injection revealed

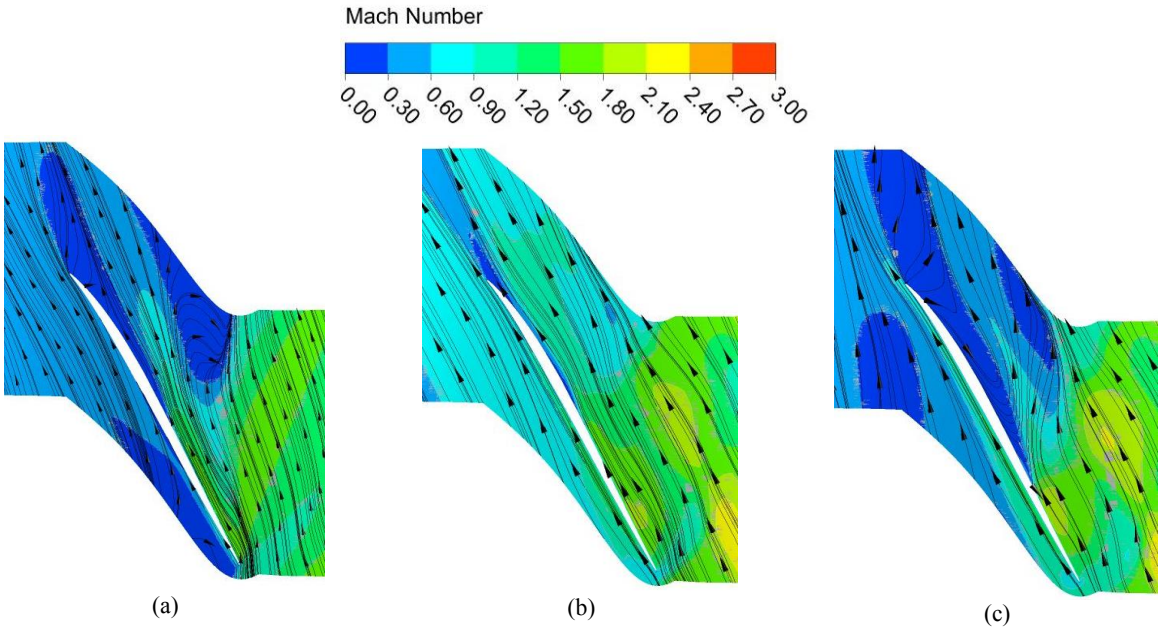

Fig. 15. The Mach number flow lines in 0.98% span (a) without injection in the performance state of A (b) with injection at the performance state of A (c) with injection at the performance state of B

the occurrence of a tip leakage vortex and a reduction in axial velocity near the leading edge due to the power of the tip leakage flow compared to the main flow. This phenomenon caused the vortex flow and strong recursive flow in this area. The states of 1 (the leading edge) to 5 (the trailing edge) are shown in order of constant streamwise location (CSL) percentage, namely 31.5%, 35.2%, 36%, 43%, and 49.5%.

In the model without injection, vorticity and significant differences do not occur. Also, in the model by injecting cases where vorticity and difference are visible are magnified. According to Fig. 14, it is clear that in the case of no injection in the tip area and the blade tip clearance, due to the strength of the tip leakage flow and its collision with the main flow in near-stall conditions, a reverse flow is created and tip leakage vortices occur. Parts of the contours where these vertices occur are zoomed in. It is known that by applying the injection, the injection flow increases the momentum of the main flow compared to the tip leakage flow and prevents the separation of the flow and the occurrence of tip leakage vortices.

Fig. 15 illustrates the flow lines at the 98% span for both states of no injection and the optimal injection state (injection intensity of 2.6%, diameter of 3mm, injection angle of 30 degrees, and distance ratio of 41.17%) at the performance state of A, at different planes along the flow. In Fig. 15a, it is evident that the Mach number abruptly changes to near-stall conditions without air injection (state A), resulting in shock waves at the inlet of the blade. Comparing the Mach contour in the injection state (15b) with the absence of the injection state (15a) at the performance point of A reveals the removal of shock waves and a significant reduction in the Mach number in the injection state. Moreover, the absence of recursive flow in the flow lines due to the application of injection prevents the formation of stall cells. It is observed that in the absence of an injection state (15a), reducing the mass flow rate leads to a stall state (performance point A) and causes the shock waves to move upward from the trailing edge, approaching the leading edge. This phenomenon causes a decrease in flow and an increase in entropy. Fig. 15c shows that the application of injection at the performance point of A removes the presence of recursive flows. However, at the performance point of B, the recursive flows reappear. In other words, applying injection causes the compressor to operate at lower mass flow rates, which is normally outside of its typical operational range.

It is clear that in the case of no injection, in near-stall conditions, the tip leakage flow becomes stronger. In other words, as the flow rate decreases, the flow angle to the blade increases. Due to the presence of a reverse pressure gradient that exists naturally in compressors and also the occurrence of a shock wave in this rotor (caused by a relative Mach higher than one), the probability of flow reversal and the occurrence of tip leakage vortex increases. This is quite clear in Fig. 15-a. The interaction of the tip leakage flow and the main flow has caused the tip leakage vortex. In addition, it is clear that due to the strength of the tip leakage flow, blockage in the main flow

occurred near the leading edge. According to Fig.s 14 and 15, it is clear that the stall cell created in the passage is developed in the circumferential and radial directions. Accordingly, the performance of the compressor is weakened in this case. By applying flow injection (Fig. 15b), it can be seen that by increasing the power of the main flow and removing the areas with low momentum, no reverse flow is created and the tip leakage vortex and stall cells are not created.

4- Conclusion

This article presents a numerical study on the effects of injection parameters as an active control method on the overall performance of the NASA Rotor 37 compressor. The results indicate that increasing the injection intensity up to 2.6% enhances both SM and SRE. However, further increasing the flow rate ratio up to 3.47% leads to a reduction in these parameters. The same trend is observed for other injection parameters as well. Specifically, increasing the injection angle up to 30 degrees improves both SM and SRE, while further increasing the injection angle up to 38 degrees results in a decrease in these parameters. Similarly, the trend of SM and SRE increases up to a distance ratio of 41.17%, but this trend shifts to a decrease at a distance ratio of 61.82%Furthermore, the study showed that changes in the distance ratio have a greater impact on the compressor performance than changes in the flow rate ratio. Additionally, among the various injection parameters, changes in the injection diameter have the least effect on the compressor performance. Based on the results, the optimal injection state for extending the stable range and increasing the stall margin is achieved with an injection intensity of 2.6%, a 3mm injection diameter, a 30-degree injection angle, and a 41.17% distance ratio. The study also revealed that in this optimal injection state, the stall margin and stable range extension increase up to 27% and 192%, respectively. The study revealed that in the injection state, there was a significant reduction in shock waves and Mach number. Additionally, the problem of drop occurrence and stall cell formation was greatly reduced. Moreover, the application of flow injection in the shell led to a decrease in shock waves and the power of tip leakage flow, resulting in a reduction in the power of the tip leakage vortex.

Nomenclature

$\dot{M}$	Injection mass flow rate ، kg/s
D	diameter ، mm
l	Distance ،mm
$\dot{m}$	Mass flow rate ، kg/s
θ	angle ، degree
μ_t	Turbulent viscosity coefficient ، kg.m-s
μ_l	viscosity coefficient ،kg.m-s
E	Total energy ، (j)
ρ	density ، $(\frac{kg}{m3})$
P	Pressure ، (pa)
F	Foreign forces entering the system ، (N)
u_i	Velocity in the xi direction ، (m/s)
u_j	Velocity in the xj direction ، (m/s)
x_i	Flow direction axis
T	temperature ، (k)
Pr	Prantel number Calm
Pr_t	turbulent Prantel numbers
τ_{ij}	Viscous stress tensor
s_{ij}	Strain rate tensor
H	Total enthalpy ، j
K	turbulent kinetic energy
ω	Turbulence-specific dissipation rate
D	Distance ،m
Ω	Indicates the magnitude of the vortex
σ_k	*Constant coefficient*
σ_ω	*Constant coefficient*
β	*Constant coefficient*
c_ω	*Constant coefficient*
a_1	*Constant coefficient*
φ_1	*Constant coefficient*
φ_2	*Constant coefficient*
f_1	*Effective diffusion function k*
f_2	*Effective diffusion function w*
Γ_1	*Effective diffusion k*
Γ_2	*Effective diffusion w*
δ_{ij}	unit tensor
s_{ij}	Shear rate tensor
P_k	Represents term k
P_ω	Represents term w

References

[1] K. Yamada, H. Kikuta, K.-i. Iwakiri, M. Furukawa, S. Gunjishima, An Explanation for Flow Features of Spike-Type Stall Inception in an Axial Compressor Rotor, in: ASME Turbo Expo 2012: Turbine Technical Conference and Exposition, 2012, pp. 2663-2675.

[2] C.-T. Dinh, M.-W. Heo, K.-Y. Kim, Aerodynamic performance of transonic axial compressor with a casing groove combined with blade tip injection and ejection, Aerospace Science and Technology, 46 (2015) 176-187.

[3] R.D. Moore, Performance of single-stage axial-flow transonic compressor with rotor and stator aspect ratios of 1.19 and 1.26 respectively, and with design pressure ratio of 2.05, National Aeronautics and Space Administration, 1980.

[4] S. Abbasi, A. Pirnia, R. Taghavi-Zenouz, Investigation of inlet distortion effects on axial compressor performance based on streamline curvature method, Journal of Theoretical and Applied Mechanics, 56(4) (2018) 1005-1015.

[5] S. Abbasi, A. Joodaki, Effect of blade profile on the performance characteristics of axial compressor in design condition, Journal of Computational & Applied Research in Mechanical Engineering (JCARME), 9(2) (2020) 287-296.

[6] S. Abbasi, A. Gholamalipour, Parametric study of injection from the casing in an axial turbine, Proceedings of the Institution of Mechanical Engineers, Part A: Journal of Power and Energy, 234(5) (2020) 582-593.

[7] C. Hah, Effects of double-leakage tip clearance flow on the performance of a compressor stage with a large rotor tip gap, Journal of Turbomachinery, 139(6) (2017) 061006.

[8] X. Ren, C. Gu, A numerical study on the tip clearance in an axial transonic compressor rotor, Applied Thermal Engineering, 103 (2016) 282-290.

[9] D. Wisler, Loss reduction in axial-flow compressors through low-speed model testing, in, Citeseer, 1984.

[10] M.W. Wiseman, T.-H. Guo, An investigation of life extending control techniques for gas turbine engines, in: Proceedings of the 2001 American Control Conference. (Cat. No. 01CH37148), IEEE, 2001, pp. 3706-3707.

[11] I. Wilke, H.-P. Kau, G. Brignole, Numerically aided design of a high-efficient casing treatment for a transonic compressor, in: Turbo Expo: Power for Land, Sea, and Air, 2005, pp. 353-364.

[12] R. Davis, J. Yao, Axial compressor rotor flow structure at stall-inception, in: 44th AIAA Aerospace Sciences Meeting and Exhibit, 2006, pp. 419.

[13] M. Zhang, A. Hou, Investigation on stall inception of axial compressor under inlet rotating distortion, Proceedings of the Institution of Mechanical Engineers, Part C: Journal of Mechanical Engineering Science, 231(10) (2017) 1859-1870.

[14] J.J. Adamczyk, M. Celestina, E. Greitzer, The role of tip clearance in high-speed fan stall, (1993).

[15] I. Wilke, H.-P. Kau, A numerical investigation of the flow mechanisms in a HPC front stage with axial slots, in: Turbo Expo: Power for Land, Sea, and Air, 2003, pp. 465-477.

[16] M. Howard, S. Gallimore, Viscous throughflow modeling for multistage compressor design, (1993).

[17] C. LeJambre, R. Zacharias, B. Biederman, A. Gleixner, C. Yetka, 1995 ASME Gas Turbine Award Paper: Development and Application of a Multistage Navier–Stokes Flow Solver: Part II—Application to a High-Pressure Compressor Design, (1998).

[18] M. Banjac, M.V. Petrovic, A. Wiedermann, Secondary flows, endwall effects, and stall detection in axial compressor design, Journal of Turbomachinery, 137(5) (2015) 051004.

[19] A. Sadagopan, C. Camci, A design strategy for a 6: 1 supersonic mixed-flow compressor stage, Aerospace Science and Technology, 87 (2019) 265-277.

[20] J. Luo, Design optimization of the last stage of a 4.5-stage compressor using a POD-based hybrid model, Aerospace Science and Technology, 76 (2018) 303-314.

[21] N. Tahara, M. Kurosaki, Y. Ohta, E. Outa, T. Nakakita, Y. Tsurumi, Early stall warning technique for axial flow compressors, in: Turbo Expo: Power for Land, Sea, and Air, 2004, pp. 375-384.

[22] M. Dhingra, Y. Neumeier, J. Prasad, A. Breeze-Stringfellow, H.-W. Shin, P.N. Szucs, A stochastic model for a compressor stability measure, in: Turbo Expo: Power for Land, Sea, and Air, 2006, pp. 833-843.

[23] Y. Liu, M. Dhingra, J. Prasad, Correlation measure-based stall margin estimation for a single-stage axial compressor, (2012).

[24] A. Young, I. Day, G. Pullan, Stall warning by blade pressure signature analysis, Journal of Turbomachinery, 135(1) (2013) 011033.

[25] F. Li, J. Li, X. Dong, Y. Zhou, D. Sun, X. Sun, Stall-warning approach based on aeroacoustic principle, Journal of Propulsion and Power, 32(6) (2016) 1353-1364.

[26] M.D. Hathaway, Passive endwall treatments for enhancing stability, 2007.

[27] S. Xiaofeng, D. Xu, S. Dakun, Recent development of casing treatments for aero-engine compressors, Chinese Journal of Aeronautics, 32(1) (2019) 1-36.

[28] J. Li, J. Du, C. Nie, H. Zhang, Review of tip air injection to improve stall margin in axial compressors, Progress in aerospace sciences, 106 (2019) 15-31.

[29] H. Chen, X. Huang, K. Shi, S. Fu, M. Ross, M.A. Bennington, J.D. Cameron, S.C. Morris, S. McNulty, A. Wadia, A computational fluid dynamics study of circumferential groove casing treatment in a transonic axial compressor, Journal of Turbomachinery, 136(3)

(2014) 031003.

[30] T.-D. Vuong, K.-Y. Kim, C.-T. Dinh, Recirculation-groove coupled casing treatment for a transonic axial compressor, Aerospace Science and Technology, 111 (2021) 106556.

[31] J. Li, J. Du, F. Li, Q. Zhang, H. Zhang, Stability enhancement using a new hybrid casing treatment in an axial flow compressor, Aerospace science and technology, 85 (2019) 305-319.

[32] A. Epstein, J.F. Williams, E. Greitzer, Active suppression of aerodynamic instabilities in turbomachines, Journal of Propulsion and Power, 5(2) (1989) 204-211.

[33] C. Koch, L. Smith Jr, Experimental evaluation of outer case blowing or bleeding of single stage axial flow compressor. Part 4-Performance of bleed insert conFig. uration no. 3, 1968.

[34] C. Koch, L. Smith Jr, Experimental evaluation of outer casing blowing or bleeding of single stage axial flow compressor. Part 2-Performance of plain casing insert conFig.uration with undistorted inlet flow and boundary layer trip, 1968.

[35] C. Nie, Z. Tong, S. Geng, J. Zhu, W. Huang, Experimental investigations of micro air injection to control rotating stall, Journal of Thermal Science, 16 (2007) 1-6.

[36] H. Khaleghi, Effect of discrete endwall recirculation on the stability of a high-speed compressor rotor, Aerospace Science and Technology, 37 (2014) 130-137.

[37] X. Liu, J. Teng, J. Yang, X. Sun, D. Sun, C. He, J. Du, Calculation of stall margin enhancement with micro-tip injection in an axial compressor, Journal of Fluids Engineering, 141(8) (2019) 081109.

[38] J. Li, Self-adaptive stability-enhancing technology with tip air injection in an axial flow compressor, Journal of Turbomachinery, 139(1) (2017) 011008.

[39] I.B.Y. Ce, Steady air injection flow control parameters in a transonic axial compressor, Research Journal of Applied Sciences, Engineering and Technology, 5(4) (2013) 1441-1448.

[40] J. Li, J. Du, Z. Li, F. Lin, Stability enhancement with self-recirculating injection in axial flow compressor, Journal of Turbomachinery, 140(7) (2018) 071001.

[41] W. Wei, C. Wuli, H. Zhang, H. Kuang, Experimental and numerical study of tip injection in a subsonic axial flow compressor, Chinese Journal of Aeronautics, 30(3) (2017) 907-917.

[42] B. Beheshti, B. Farhanieh, K. Ghorbanian, J. Teixeira, P. Ivey, Performance enhancement in transonic axial compressors using blade tip injection coupled with casing treatment, Proceedings of the Institution of Mechanical Engineers, Part A: Journal of Power and Energy, 219(5) (2005) 321-331.

[43] B.H. Beheshti, K. Ghorbanian, B. Farhanieh, J.A. Teixeira, P.C. Ivey, A new design for tip injection in transonic axial compressors, in: Turbo Expo: Power for land, sea, and air, 2006, pp. 39-47.

[44] A. Mushtaq, K. Parvez, S. Ahmad, J. Khan, Parametric study of tip injection on stability of transonic axial flow compressor, in: 49th AIAA Aerospace Sciences Meeting including the New Horizons Forum and Aerospace Exposition, 2011, pp. 744.

[45] L. Reid, R.D. Moore, Design and overall performance of four highly loaded, high speed inlet stages for an advanced high-pressure-ratio core compressor, 1978.

[46] G. Cassina, B.H. Beheshti, A. Kammerer, R.S. Abhari, Parametric study of tip injection in an axial flow compressor stage, in: Turbo Expo: Power for Land, Sea, and Air, 2007, pp. 137-145.

[47] J. Li, F. Lin, Z. Tong, C. Nie, J. Chen, The dual mechanisms and implementations of stability enhancement with discrete tip injection in axial flow compressors, Journal of Turbomachinery, 137(3) (2015) 031010.

[48] M.D. Hathaway, Self-recirculating casing treatment concept for enhanced compressor performance, 2002.

HOW TO CITE THIS ARTICLE

S. Abbasi, M Raiszadeh Oskoui , Investigating the Effect of Casing Injection Parameters on Transonic Axial Compressor Performance, AUT J. Mech Eng., 7(4) (2023) 367-388.

DOI: 10.22060/ajme.2024.22716.6071